Supplementary Information

Compositional effects on $D^N_{m/s}$ values

We completed individual series of experiments to quantify compositional controls on nitrogen partitioning. Each series is detailed here.

Carbon-nitrogen interactions in liquid Fe alloy:

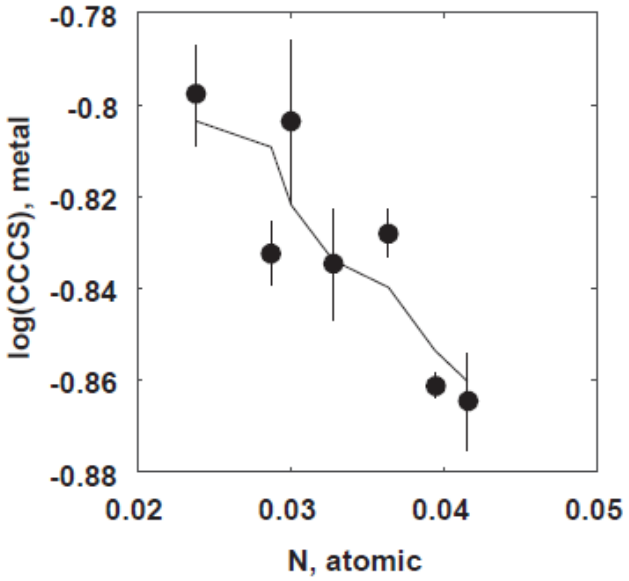

Supplementary Figure 1: Correlation between N and C concentration in Fe alloys at graphite saturation (N series). The negative correlation between N and C concentrations indicate that N and C repel each other in liquid Fe alloy. The solid line is the predicted relationship between N and C concentrations using an interaction parameter of 5.9±1.9.

We conducted a series of experiments (N series) with variable X^N_{metal} to quantify the effect of N on C solubility in Fe alloy (Supplementary Figure 1). Measured X^C_{metal} values are treated as solubility because the experiments were completed in graphite capsules, fixing *a*C to unity. The correlation between X^C_{metal} and $X^{\varepsilon N}_{metal}$ is fit with a ε^C_N value of 5.9 ± 1.9 (R^2 = 0.7, p-

value = 0.02, n = 7). The non-smooth model fit reflects that N series experiments were conducted under variable temperatures, and lower temperatures correspond with a stronger N-C interaction in Fe alloy.

P-T-X conditions of the N series are nearly constant at 0.95 GPa, 1773-2173 K, and IW-1.6 to IW-1.8. The negative relationship between carbon solubility and X_{metal}^{N} is qualitatively constant with results from the steel making literature [51] and recent N solubility work [e.g., 22,26]. We use the ε_N^C value to correct all experiments to C-free baseline for further fitting using the following equation (Eq. 8)

$$\ln\left(D_{m/s}^{N,C\ free}\right) = \ln\left(D_{m/s}^{N}\right) - \varepsilon_N^C \times X_{metal}^{\varepsilon C}$$

Oxygen fugacity

Oxygen fugacity ($f\mathrm{O_2}$) is a major control on how volatile elements speciate, and each species will have its own unique partitioning behavior during core formation. We conducted a series of isothermal and isobaric experiments (1973 K and 0.95 GPa) to define the relationship between $f\mathrm{O_2}$ and $D_N^{m/s}$ (Figure 3a). Data between ΔIW-5 and ΔIW-1 define a positive relationship between $f\mathrm{O_2}$ and $\log_{10}(D_N^{m/s})$, where $\log_{10}\left(\boldsymbol{D_{m/s}^{N}}\right) \propto 0.64 \pm 0.09\Delta IW$ or $\ln\left(\boldsymbol{D_{m/s}^{N}}\right) \propto 1.48 \pm 0.22\Delta IW$. This individual series correlation coefficient within error of the coefficient determined for the global regression (1.38 ± 0.14). A similar relationship between $f\mathrm{O_2}$ and $D_{m/s}^{N}$ has been documented in the literature [e.g., 23,26].

The role of $f\mathrm{O_2}$ in controlling $D_{m/s}^{N}$ values can be understood in terms of changes in N solubility within silicate melt. It has been established that reducing conditions stabilize nitride

species in silicate melt, increasing N solubility proportional to $fO_2^{-3/4}$ according with the following reaction:

$$N^{-3} + \frac{3}{4}O_2 = \frac{3}{2}O^{-2} + \frac{1}{2}N_2$$

(Eq. 7)

A $\log_{10}$ coefficient of 0.64±0.09 is within error of the theoretical 0.75 value. A lower than theoretical slope may suggest the N content of metal also has a small fO_2 dependence or small deviations from Henrian solution behavior of N in melt or that nitrogen species with an oxidation state intermediate to N_2 and N^{-3} influence melt solubility.

Under extremely reducing conditions (<ΔIW-5) there is preliminary evidence for a new $D^N_{m/s} - fO_2$ regime (Figure 3a). This shallowing may indicate that nitride species are fully stabilized, such that changes in fO_2 no longer lead to changes in N solubility in silicate melt. Indeed, measurements of nitrogen solubility in silicate liquid below ΔIW-6 (1 atmosphere and 1698 K) appear to plateau relative to solubility measurements under more oxidized conditions [8].

Effect of nickel

We conducted a series of experiments to constrain the effect of Ni in modulating $D^N_{m/s}$ values. Pressures and temperatures were held constant at 0.95 GPa and 1973 K. The individual series correlation yields a ε_N^{Ni} value of 5.3 ± 1.8 (R^2 = 0.95, p-value = 0.02, n = 4). This value is within error of those determined in the global regression (ε_N^{Ni} = 5.0 ± 1.1). The negative effect of Ni on $D^N_{m/s}$ values is qualitatively consistent with literature results [20]. ;

Effects of S and ionic porosity

We conducted series of experiments to constrain the effects of sulfur and ionic porosity on nitrogen partitioning. These two effects are not included in Eq. 1 because the effect of S in our dataset is not significant at the 95% confidence threshold and the applicability of low pressure ionic porosity results to high pressure systems has not been demonstrated.

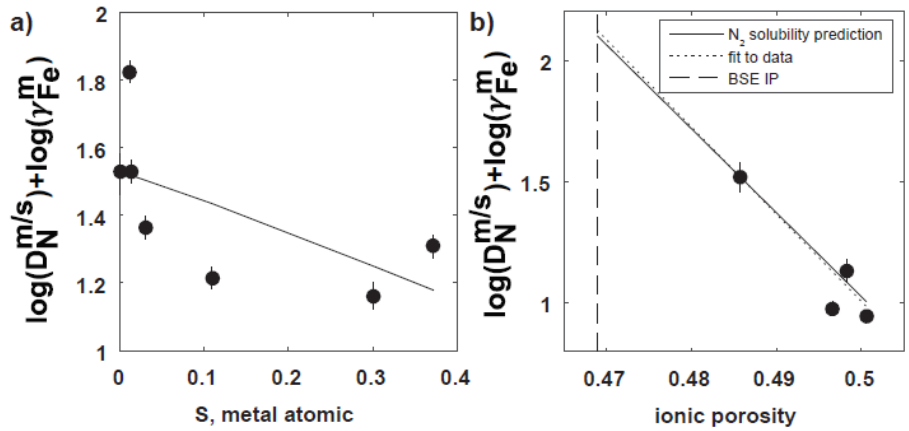

Supplementary Figure 2: Other compositional effects on nitrogen partitioning. a) The effect of sulfur on nitrogen partitioning. All partitioning values have been corrected to a common set of conditions to isolate the effects of compositional parameters (T=1973 K, P=1 GPa, IW = -2, $X^{metal} = 0$) using the parameters in Eq. 1 and the ε^C fit in Supplementary Figure 1. b) The effect of ionic porosity on nitrogen partitioning. Experiments were run at 1 GPa and 1973 K, and all data have been corrected to IW-2. The solid line is a least squares fit to the partitioning data, and the dotted line is a model prediction for nitrogen partitioning values assuming ionic porosity increasing the solubility of N in melt following the established behavior for Ar (Carroll and Stolper, 1993). The model is forced through the low ionic porosity data point. The vertical dashed line is the ionic porosity for a bulk silicate Earth liquid.

Within the S series, temperatures varied between 1973 and 2413 K and pressures varied between 0.95 and 2.38 GPa (Supplementary Figure 2a). We varied pressure and temperature to provide a greater range of X_{metal}^S values within the S series. The addition of S to Fe alloy apparently makes N less siderophile but the correlation is not significant. Fitting the S series yields a ε_N^S value of 1.9 ± 1.1 (R^2 = 0.42, p-value = 0.12, n = 7). The negative effect of S on $D_{m/s}^N$ values is qualitatively consistent with literature results [25].

We explored the effect of ionic porosity on $D_{m/s}^N$ value because it is well-established that ionic porosity controlled the solubility of neutral species, such as N_2, in silicate melt. More

silica-rich liquids have greater ionic porosity and should consequently have a higher N solubility, provided that N solubility is dominated by neutral species. This behavior will translate into a higher concentration of N in magma in equilibrium with liquid metal, and a lower $D^N_{m/s}$ value. We test for this effect by completing N partitioning experiments with higher ionic porosity silicate liquids compared to the basaltic liquid used in the remaining piston cylinder experiments (Supplementary Figure 2b). The solubility of N_2 is very similar to Ar in magma due to their equal charge and similar radius, and we use established correlations between Ar solubility and ionic porosity [54] to predict the sensitivity of $\log(D^N_{m/s}) + \log(\gamma^{Fe}_{metal})$. High ionic porosity experiments do have lower corresponding $\log(D^N_{m/s}) + \log(\gamma^{Fe}_{metal})$ (recalculated to carbon free baseline and to IW-2), and the magnitude is well predicted by the predicted ionic porosity sensitivity. These experiments provide preliminary evidence that ionic porosity modulates $D^N_{m/s}$values and that N_2 is the melt dominant species within the ionic porosity series. Magma oceans have low ionic porosity related to their ultramafic composition, but extrapolating this effect from our 1 GPa experiments to deep magma oceans, however, is difficult due to the collapse of melt structure with pressure. We do not include this effect in Eq. 1 for this reason.

The apparent influence of both ionic porosity and fO_2 on $D^N_{m/s}$ values suggests that N speciation in PC series experiments is in a mixed regime where both nitride and N2 contribute to melt solubility.

Validation of predictive power of Eq 1.

We combine the individual series (*1/T, P/T,* X^{Ni}_{metal}, ΔIW) into a global dataset and conduct a multiple least squares regression to predict $D^{N,C\,free}_{m/s}$ values up to the *P-T* conditions associated with average core formation within Earth (Eq. 1). Supplementary Figure 3a plots the

1:1 correlation between observed and predicted $\log(D^N_{m/s}) + \log(\gamma^{Fe}_{metal})$ values. We note that in the absence large amounts of alloying elements, γ^{Fe}_{metal}value are near zero.

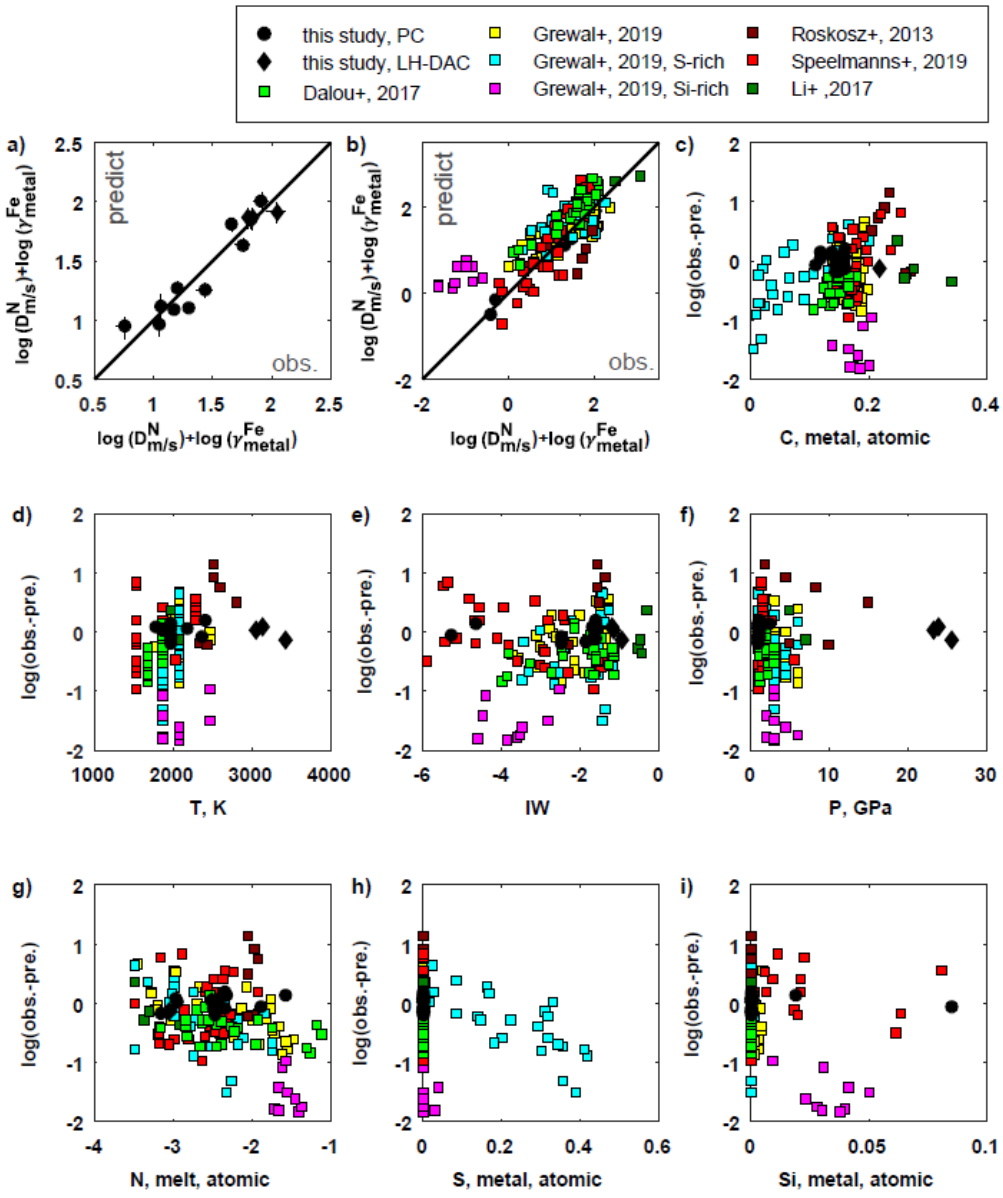

Supplementary Figure 3: Comparison of nitrogen partitioning predicted by Eq. 1 and observed values in a) this study and b-i) the literature. All data have been recalculated to a C-free baseline. Eq. 1 predicts literature data with an R^2 value of 0.82 not including the experiments with S-rich and Si-rich Fe alloy from Grewal+ (2019).

To validate the predictive power of Eq. 1, we compare $D^N_{m/s}$ reported in the literature [20,22,23,25,26] to values predicted from the associated experimental conditions and chemical analyses

(Supplementary Figure 3b-i). Data were collected over a relatively wide range of conditions: 1523 to 2800 K, 0.85 to 14.8 GPa, -0.3 to -5.9 ΔIW). All literature $D^N_{m/s}$ values are recalculated to a carbon-free baseline (Eq. 8), and then we apply Eq. 1 to their corresponding experimental conditions to predict the $D^N_{m/s}$ value for the experiment. Our comparison yields an R^2 value of 0.82. We stress that we simply predict the literature data, as Eq. 1 was derived only from the experiments reported here, rather than fit the literature data. Study *20* only reports carbon for a subset of their experiments, and for experiments without carbon analysis, we assume the average carbon concentration from their reported values.

The higher pressure data available are consistent with a relatively strong, positive effect of pressure on $D^N_{m/s}$ values (Supplementary Figure 3f). We not compare with experiments that contain sulfur, as Eq. 1 does not account for any potential sulfur effect and there is evidence that sulfur can decrease $D^N_{m/s}$ values (*25*, Supplementary Figure 2a). Indeed, fitting residuals correlate with S content (Supplementary Figure 3h). We also do not compare with the experiments that contain alloy with elevated Si contents (>0.5 wt %) from *25*, as the fitting residuals for these data are systematically offset other experiments with Si-bearing alloys conducted at similar fO_2 (Supplementary Figure 3i).

Validation of pressure and temperature determinations of LH-DAC experiments

We use the partitioning of Ni, Mg, Si between metal and silicate to verify the accuracy of the *P-T* conditions of our LH-DAC experiments, as partitioning of these elements are relatively strong functions of pressure and temperature (Supplementary Figure 4). We compare our $D^{Ni-Fe}_{m/s}$ data (filled black circles) to the compiled data from *29* (open squares) (Supplementary Figure 4a). All $D^{Ni-Fe}_{m/s}$ data are recalculated to infinite temperature to isolate the effect of

pressure using the temperature dependency reported by *29*. We compare our $D_{m/s}^{Mg}$ data to the compiled data from *53* in Supplementary Figure 4b. All $D_{m/s}^{Mg}$ data are recalculated to O-, C-, S-, and Si-free metal compositions using the dependencies reported by *53* to isolate the effect of temperature. We additionally compare our $D_{m/s}^{Si-Fe}$ data to the compiled *29* in Supplementary Figure 4c. All $D_{m/s}^{Si-Fe}$ data are recalculated to O-, C-, and N-free metal compositions using the dependencies reported by *29* (O and C) and *51* (N).

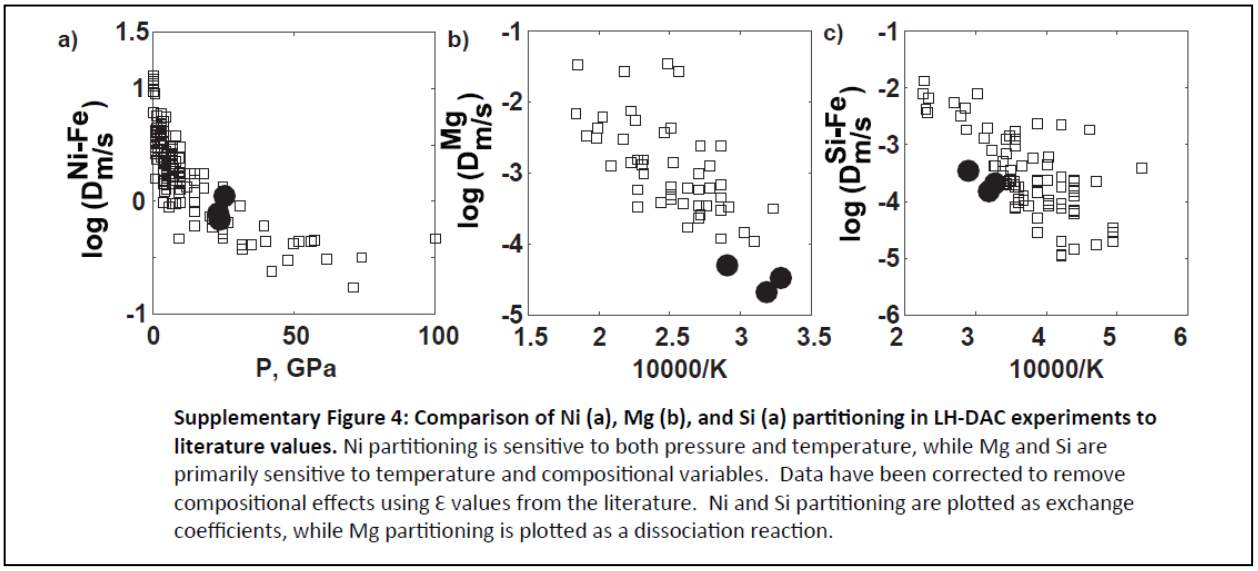

Supplementary Figure 4: Comparison of Ni (a), Mg (b), and Si (a) partitioning in LH-DAC experiments to literature values. Ni partitioning is sensitive to both pressure and temperature, while Mg and Si are primarily sensitive to temperature and compositional variables. Data have been corrected to remove compositional effects using ε values from the literature. Ni and Si partitioning are plotted as exchange coefficients, while Mg partitioning is plotted as a dissociation reaction.

Agreement between our major element partitioning data and the literature data is good for Ni and Mg. Our data do plot near on the left edge of the $D_{m/s}^{Si-Fe}$ literature data field. Given the good agreement for the Mg dataset, which suggests accurate temperature measurements, the offset within the Si dataset may suggest 1) minor accuracies in the measurement of the Si content of metals in our experiments and/or 2) the underestimation of the effect C in lowering $D_{m/s}^{Si-Fe}$ values, given the relatively C-rich nature of the metal phases in our experiments (Supplementary Table 1).

Parameterization of $D_S^{m/s}$ values

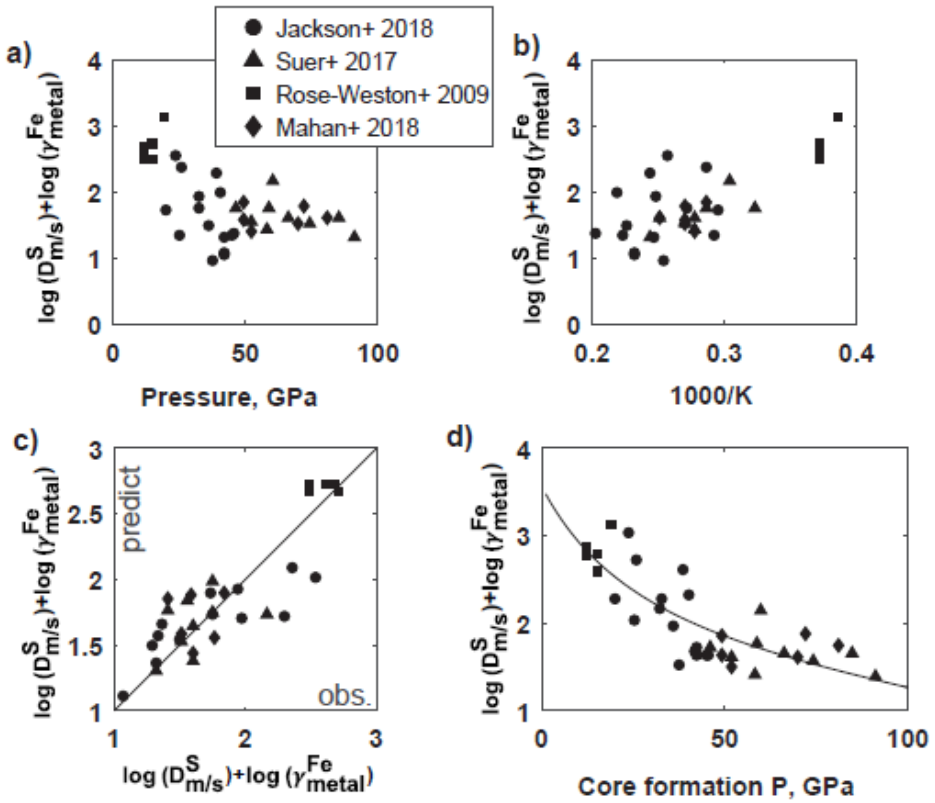

Supplementary Figure 5: Parameterization of S partitioning. Correlations with a) pressure and b) inverse temperature used to parameterize S partitioning (Eq. 2). c) A comparison of observed and predicted values. d) Application of Eq. 2 to the mantle liquidus geotherm. Partitioning data are offset from the model by the difference between their measured value and their value predicted by Eq. 2. Sulfur is decreasingly siderophile with more extreme core formation *P-T* conditions.

We take data collected from experiments run over 10 GPa from *18* and *30-32* to parameterize $D^S_{m/s}$ values (Supplementary Figure 5). Lower pressure data are not included because their extrapolation to higher *P-T* values is inconsistent with more newly made observations. Our base model includes a constant term and following variables: $\frac{1}{T}, \frac{P}{T}, \ln(aFeO), \ln(C_S)$ and $X^{\varepsilon C}_{metal}$. The C_S term is the sulfur content at sulfide saturation. The $\frac{1}{T}, \frac{P}{T}$ and constant terms are added to the model and a stepwise approach is used to determine if any of the compositional parameters are significant. We identify $X^{\varepsilon C}_{metal}$ as the only significant additional parameter, which is fit with an ε^C_S value of 11.0 ± 1.0. This fit $\boldsymbol{\varepsilon}$ parameter is similar

to the ε_S^C value from the steelmaking literature [51]. The partitioning of sulfur should also be affected by the capacity of the silicate liquid to complex with S^{-2} ions. To test if this effect is significant in the current dataset, we introduce the $\ln(aFeO)$ and $\ln(C_S)$ terms into the stepwise matrix. The coefficients for both terms are negative, as anticipated, but neither is significant (p-values of 0.23 and 0.26, respectively) and are not included in the final model.

Primordial differentiation models with variable core oxygen content, disequilibrium, and alternative $D_{m/s}^C$ parameterization

We have developed a primordial differentiation model to highlight the dual roles of gas solubility and metal-silicate partitioning on modulating Earth's distribution of volatile elements. Here we demonstrate the sensitivity of the model to changes in the oxygen content of the core (X_{metal}^O), core-magma ocean-atmosphere disequilibrium, and taking the SIMS data parameterization of $D_{m/s}^C$ from *33***.**

Effect of core oxygen content

The $D_C^{m/s}$ parameterization we employ [33] highlights the importance of core metal oxygen content. Recent estimates for core oxygen content range from ~2 to 5 wt. % or X_O^{metal} values of ~0.05 to 0.17 [29,36].

147 We report model results for $D^{C}_{m/s}$ calculated with 0.6 and 0.12 X^{O}_{metal} applied to
148 scenarios with N-S-C ratios set by gas-poor chondrites (Supplementary Figure 6). Results for
149 0.06 X^{O}_{metal} models are plotted in Supplementary Figure 6a-c. Subtraction of oxygen from the
150 core decreases $D^{C}_{m/s}$ values and therefore forces $(C/N)_{OE}$ and $(S/C)_{OE}$ solutions to lower
151 pressures (c.f. Figure 6 and Supplementary Figure 6a-c). The solution fields for $(S/C)_{OE}$ and
152 $(S/N)_{OE}$ still overlap under oxidizing atmospheric conditions, but the amount of overlap is less
153 compared to nominal case (9 mol % O, Figure 6).

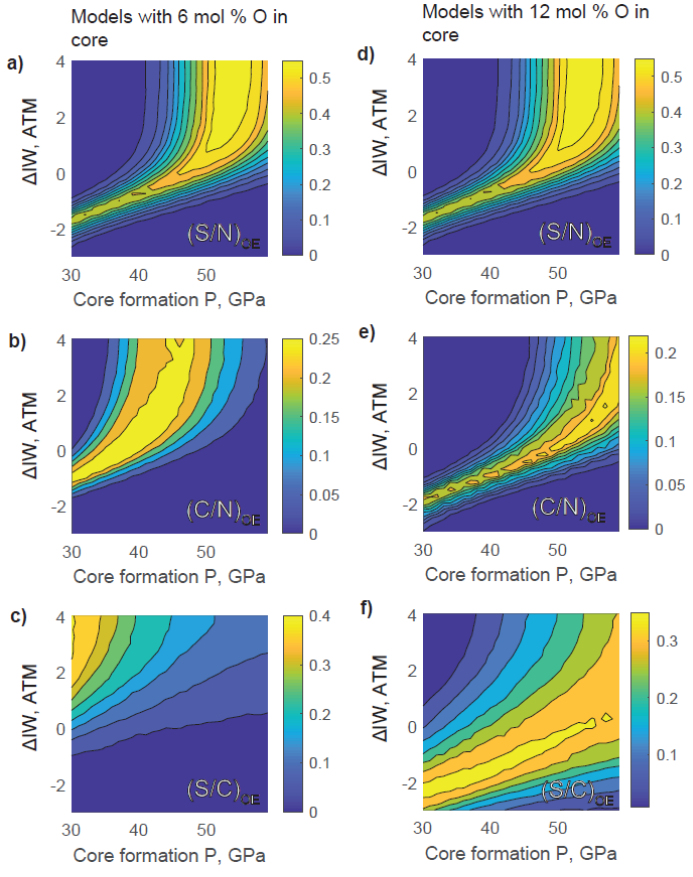

Supplementary Figure 6: Primordial differentiation models with variable oxygen concentrations in the core. a-c) Models with 6 mol % oxygen. **d-f)** Models with 12 mol % oxygen. Oxygen content only affects metal-silicate partitioning of carbon. Both sets of models were completed with N-S-C ratios set by gas-poor chondrite.

154 Results for the 0.12 X^{O}_{metal} models are plotted in Supplementary Figure 6d-f. The
155 addition of oxygen to the core increases $D^{C}_{m/s}$ values and therefore forces $(C/N)_{OE}$ and $(S/C)_{OE}$

solutions to higher pressures (c.f. Figure 6 and Supplementary Figure 6d-f). Solutions for $(S/N)_{OE}$ remain unchanged. The net consequence is that the maximum probability of $(S/N)_{OE}$, $(C/N)_{OE,}$ and $(S/C)_{OE}$ solutions converge for under a common condition of oxidizing atmospheres and relatively high pressure core formation (>50 GPa).

Effect of magma ocean-atmosphere disequilibrium

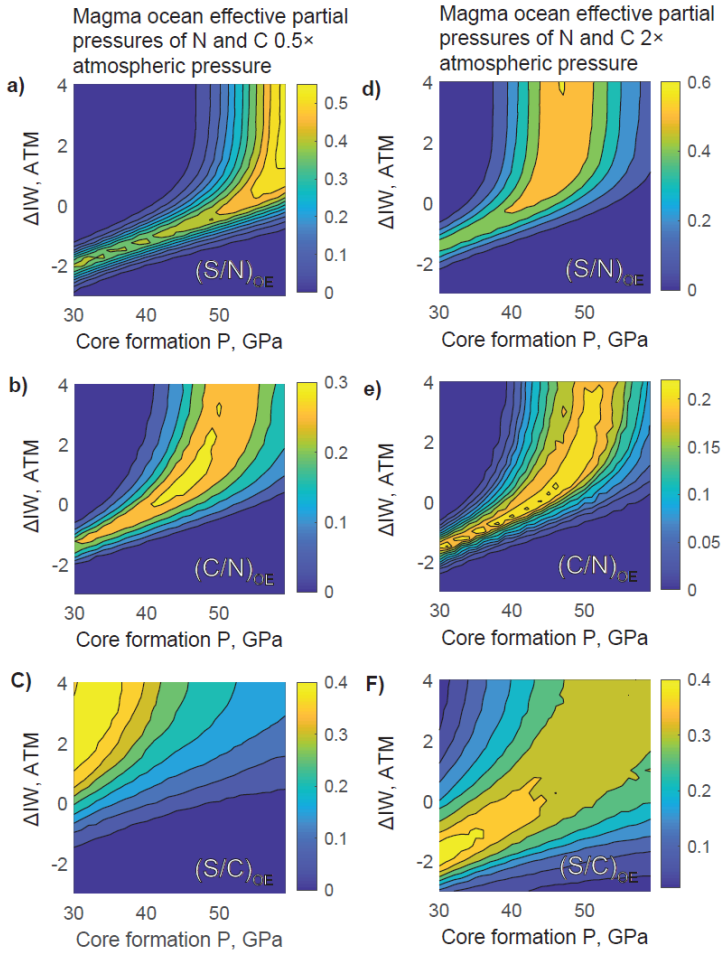

Supplementary Figure 7: Primordial differentiation models with variable effective partial pressures of N and C in the magma ocean relative to the atmosphere. a-c) Model solutions for magma ocean effective partial pressures of N and C 0.5× their values in the atmosphere. **d-f)** Is the same as A-C) but with effective partial pressures of N and C at 2× their values in the atmosphere. Both sets of models were completed with bulk planet N-S-C ratios set by gas-poor chondrite.

Stokes settling of metal in a low viscosity magma ocean suggests core formation events last <1 day. The timescale associated with exchange of volatile species between the primordial

atmosphere and overlying magma ocean is not well known, but may be >>1 day if exchange is modulated by a diffusive boundary layer with thickness >1 m [42]. It is therefore likely that equilibrium was not fully established with any core formation episode. In this case, establishing atmosphere-magma ocean equilibrium will lag behind establishing core-magma ocean equilibrium. We introduce disequilibrium into our model by allowing the effective partial pressure for N and C the magma ocean to be different than their corresponding partial pressure in the overlying atmosphere (effective partial pressure is the pressure of gas required to dissolve the concentration of that gas in magma). We envision disequilibrium manifesting in two ways. First, we consider cases where N and C have *lower* effective partial pressures in the magma ocean relative to their pressures in the overlying atmosphere (Supplementary Figure 7a-c). We then consider cases where N and C have *higher* effective partial pressures in the magma ocean relative to their pressures in the overlying atmosphere (Supplementary Figure 7d-f). All models reported in Supplementary Figure 7 assume gas-poor chondrite N-S-C ratios for the bulk planet, and Figure 6 is the nominal case, where equilibrium is assumed between the magma ocean and atmosphere.

The *low* effective partial pressures models (Supplementary Figure 7a-c) have $(S/N)_{OE}$ and $(S/C)_{OE}$ solutions that are shifted to higher and lower pressures, respectively, compared to Figure 6. These shifts have the tendency to limit the core formation *P*-atmospheric fO_2 space where N-S-C ratios are mutually satisfied, although maximum solution over occurs for relatively oxidizing atmospheres.

The *high* effective partial pressure models (Supplementary Figure 7d-f) have $(S/N)_{OE}$ and $(S/C)_{OE}$ solutions to lower and higher pressures, respectively, compared to Figure 6. Higher

concentrations of N and C in the magma ocean makes the core also a proportionally larger reservoir for these elements, given a fixed metal-silicate partition coefficient.

Effect of using SIMS data parameterization of $D_C^{m/s}$ values

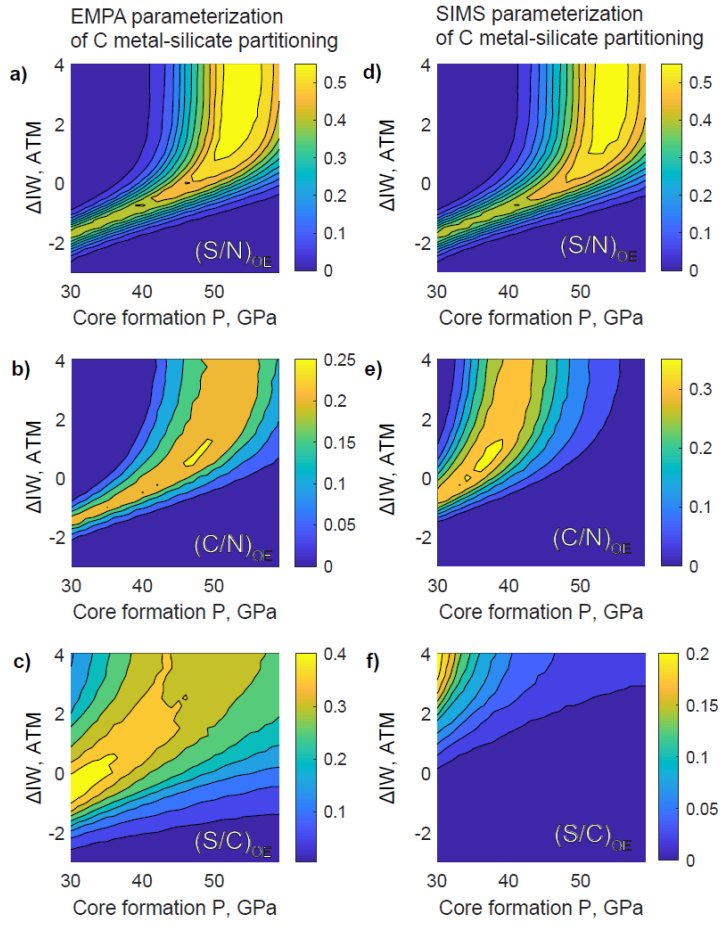

Supplementary Figure 8: Equilibrium primordial differentiation model with bulk planet N-S-C ratios set by gas-poor chondite using different parameterizations of C. a-c) EMPA parameterization of 33. **d-f)** SIMS parameterization of 33. Panel A-C) are taken from Figure 5 for comparison purposes. Both sets of models were run with 9 mol % O.

Fischer et al. (2020) (*33*) report the only currently available partitioning data for C under *P-T* conditions directly applicable to average core formation conditions within Earth. They analyze their experiments by both EMPA and SIMS techniques and report $D_C^{m/s}$ values for both techniques. The respective parameterizations terms are within uncertainty, but the EMPA-based

parameterization has a nominally lower dependence on temperature and higher dependence on core oxygen content.

Supplementary Figure 8 compares model outputs that use the EPMA (a-c) and SIMS (d-f) parameterizations. The most striking difference in comparing solutions from EMPA and SIMS parameterizations is that $(S/C)_{OE}$ solutions. This result reflects carbon being less siderophile for equal *P-T-X* conditions in the SIMS data parameterization. Less siderophile C lowers predicted $(S/C)_{OE}$ ratios, which is compensated for by adjusting successful solutions to lower pressure where carbon become more strongly siderophile. Larger amounts of oxygen in the core or a relatively high effective partial pressure of carbon in the magma ocean both act to increase the retention of carbon in the core and will therefore counter the effects of assuming the SIMS data parameterization.